

THE EFFECT OF TARGET THICKNESS ON THE BALLISTIC BEHAVIOR OF HYBRID CFRP/KFRP COMPOSITES

Sai Zhao^{1,2}, Jia Huang^{1,2,3*}, Chao Zhang^{1,2**}

¹School of Civil Aviation, Northwestern Polytechnical University, Xi'an, 710072, China
 ²Shaanxi Key Laboratory of Impact Dynamics and Its Engineering Applications, Northwestern Polytechnical University, Xi'an, 710072, China
 ³Key Laboratory of Impact and Safety Engineering, Ministry of Education, Ningbo University, Ningbo 315211, Zhejiang, China

Abstract

To achieve structural lightweight and sufficient containment capability, the use of hybrid composites to civil aircraft engine cases is a major trend. One important but neglected topic was investigated that the thickness effects of hybrid carbon/Kevlar fiber-reinforced epoxy laminates on ballistic impact properties. Based on the results of ballistic impact tests, the finite element models of ballistic impact on carbon/Kevlar hybrid laminates were established using a progressive damage constitutive model, considering different thicknesses, impact faces and layering sequences. The results confirmed an extremely strong relationship between thickness and ballistic impact properties, which has never been addressed in any previous studies of composite stacking methods. Analyses further suggested that the C-K configuration, with CFRP as the impact surface and KFRP as the back surface, exhibits superior impact resistance when the thickness is relatively thin. Conversely, with thicker configurations, the K-C setup, where CFRP serves as the impact surface and KFRP as the back surface, demonstrates stronger impact resistance. This study provides theoretical support for the design and development of aero-engine cases.

Keywords: Hybrid composites; Impact behavior; Finite element analysis (FEA); Layered structures; Thickness effect.

1. Introduction

The high-bypass turbofan engine is widely used in large commercial and cargo aircraft due to its large intake area and high propulsive efficiency. However, the larger intake area of the engine also increases the likelihood of foreign object damage (FOD) to the fan blades. In the event of blade failure due to FOD or fatigue loading, the broken blade can strike the fan case due to the high centrifugal force. Therefore, the engine case not only forms the airflow passage, but also plays a critical role in preventing blade separation [1]. If the case does not have sufficient containment capability, the high-speed and high-energy debris can penetrate the case and cause catastrophic secondary damage to the aircraft, including loss of life. The regulations require the engine case to be strong enough to contain any broken or detached blade at maximum operating speed, without significant rupture or distortion that could endanger other parts of the aircraft.

With the continuous improvement of high-performance composite manufacturing technology, lightweight and high-strength impact-resistant structures made of high-performance composites have been widely used in civil aircraft engine cases [2]. The rational design of composite case structures exhibits higher tolerance than metal and significantly reduces the weight of the engine [3]. During the containment design stage of the areo-engine case, flat plate impact experiments are commonly used to determine the impact resistance of the target plate. This method has a short design iteration cycle, relatively low experimental cost, and can provide a preliminary evaluation of failure modes, deformation processes, and containment effects of the engine case [4].

Extensive research has shown that using different types of fibers to form hybrid composites is an effective way to improve the impact resistance of composite materials. By adjusting the content,

INSERT RUNNING TITLE HERE

laying method, braiding method, etc. of each fiber, a composite material with high comprehensive performance can be designed according to the requirements. Basha et al. [5] conducted impact tests with different impact energies, and the results showed that the impact resistance of carbon/Kevlar hybrid fiber laminates was significantly improved compared to all-carbon fiber laminates, and the level of damage was reduced. Gustin et al. [6] replaced one layer of carbon fiber with Kevlar fiber for low-velocity impact tests on composite laminates, and the experimental results showed that the impact performance of the hybrid laminates was improved by about 10%. Karthick et al. [7] conducted numerical studies on the impact damage of carbon/Kevlar mixed composites under high-speed projectiles, and found that hybrid composite materials can improve impact strength and ballistic limit velocity. The above literature indicates that hybridizing an appropriate amount of Kevlar fibers in carbon fibers can significantly improve the impact resistance of composite materials.

Researchers have investigated the issue of the positioning of carbon and Kevlar fiber layers in hybrid composite laminates in order to improve impact resistance. The consensus among these studies is that composite materials with good tensile properties should be placed on the back of the laminates, while those with good shear strength should be placed on the impact face. Bandaru et al. [8] found that placing Kevlar fiber layers on the rear side and carbon fiber layers on the front side of a 5mm-thick hybrid composite laminate improved its toughness and stiffness, resulting in significantly enhanced elastic resistance. Hazell et al. [9] incorporated Kevlar fabric and aluminum layers into carbon fiber-reinforced composite laminates to improve their ballistic impact resistance and found that introducing Kevlar fabric on the back face was the most effective in dissipating projectile kinetic energy. Li et al. [10] compared ballistic experiments and finite element analyses of hybrid fiber laminates to analyze the influence of fabric hybridization on ballistic impact damage and energy absorption, concluding that a carbon/Kevlar hybrid laminate with carbon layers on the front face demonstrated improved energy absorption and ballistic limits. Tanabe et al. [11] investigated the fracture behavior and energy absorption of 2mm-thick CFRP laminates made of three different types of carbon fibers at relatively high impact velocities (150-314m/s) and found that CFRP layers made of high-tensile strength fibers on the rear side could absorb more energy within this velocity range. Cheon et al. [12] optimized the stacking sequence of hybrid fibers with enhanced stab resistance through drop tower tests and suggested that CFRP with high stiffness and hardness should be placed on the surface facing the blade while AFRP with better cutting resistance and impact energy absorption should be placed on the back face. In contrast to the literature mentioned above, Grujicic [13] holds a different perspective. His research indicates that for a 25.3mm thick CFRE/KFRE laminated plate, when the KFRE laminated plate is used as the outer surface of the armor and is therefore the first to be hit by a projectile, excellent ballistic performance of the hybrid armor can be achieved. The specific mechanism behind this experimental phenomenon is not yet clear. The conflicting conclusions of previous studies indicate that some critical factors affecting the positioning of carbon/Kevlar fibers were not analyzed in the research process, and different conclusions were drawn without declaring the certainty of these factors. To the best of the author's knowledge, no related studies have reported on this critical

Based on the research findings summarized above, it can be concluded that for studies reporting better impact resistance performance of Kevlar fibers on rear side, the thickness of the target plate is generally less than 6 mm and can be considered as thin plates. In contrast, for studies showing that hybrid laminates have better impact resistance with Kevlar fibers on front side, the thickness of target plate is thicker than 20 mm. Therefore, this paper proposes the hypothesis that target plate thickness may significantly affect the Kevlar fiber putting on the front side or rear side. Previous studies have shown that different thicknesses of target plates often correspond to different impact failure mechanisms. Nguyen et al. [14] established experiments and models to determine the ballistic performance of ultra-high molecular weight polyethylene (UHMW-PE) composite materials with thicknesses ranging from 9mm to 100mm against simulated fragments with calibers of 12.7mm and 20mm. They observed that thin plates (about <10mm thick) had larger expansion and their failure mode was mainly in fiber tension. As the thickness increased, the target plate's penetration process could form two stages: initial penetration shear blockage and backplate expansion and protrusion. Gellert et al. [15] conducted ballistic impact tests on glass and Kevlar

fibers with different thicknesses and drew a perforation energy-thickness relationship chart, showing a bilinear relationship. For thin targets, the damage form was a layered cone on the back of the target plate, and the diameter and height of the cone increased with the thickness of the target material until the target plate reached a certain thickness, and the impact side also produced a layered cone. They hypothesized that this transition was due to a change in the perforation mechanism. Nunes et al. [16] studied the response of Kevlar29/epoxy laminates with different thicknesses (4.5-14.5mm) to round nose and conical projectiles through experiments and numerical methods. The main damage mechanism of thin composite materials was fiber damage, while that of thick composite materials was layering, which was also the main energy absorption mechanism. Shaktivesh et al. [17] believed that in general, the main energy absorption mechanisms were different due to the different thicknesses of the target. The deformation of the conical shape on the back of the target material and energy absorption were the characteristics of thin composite materials, while shear blockage energy absorption was the characteristic of thick composite materials. Naik et al. [18] published several papers analyzing the damage and energy absorption mechanisms of composite material target plates under impact in detail from a theoretical perspective. They pointed out that for a 19mm thick glass fiber target plate, the main energy absorption mechanism was shear blockage, which absorbed a large amount of energy by compressing and friction in the area directly below the projectile. From the above literature, it can be seen that researchers generally believe that the energy absorption mechanisms and damage mechanisms of thin and thick composite plates under impact are different. This suggests that the impact penetration mechanisms at different thicknesses may differ, resulting in differences in the energy absorption capacity of carbon or Kevlar fibers as face materials, which is defined as the thickness effect in the present paper.

In order to have a better understanding of the thickness effect exhibited in the impact resistance of carbon/Kevlar hybrid composite materials, this study fabricated hybrid fiber composite laminates with different hybridization patterns using the Advanced Placed-PLY (AP-PLY) method. Ballistic impact tests were conducted to obtain the penetration velocity and damage form of the laminates with different staking sequences. A simulation model of the AP-PLY laminates in the commercial finite element program ABAQUS® was established and a progressive damage constitutive model was implemented to simulating the impact damage of composite laminates in a user-defined material model (VUMAT) with the consideration of strain rate effects. Hashin and Hou failure criteria was used as the damage initiation criteria, and Murakami-Ogino damage theory was utilized the to establish a damage evolution model for stiffness reduction. Two element deletion methods were parallelly used to delete failed elements. In the simulation model, carbon fibers and Kevlar fibers were in a double-layer stacking form, and the Kevlar fiber mass fraction was determined to be 25%. Numerical tests were conducted on the laminate with different thicknesses (1mm-19mm) impacted by titanium alloy bullet with high velocity from both front and rear sides to study the mechanism of aforementioned thickness effect. In order to have a better understanding of the thickness effect exhibited in the impact resistance of carbon/Kevlar hybrid composite materials, this study fabricated hybrid fiber composite laminates with different hybridization patterns using the Advanced Placed-PLY (AP-PLY) method. Ballistic impact tests were conducted to obtain the penetration velocity and damage form of the laminates with different staking sequences. A simulation model of the AP-PLY laminates in the commercial finite element program ABAQUS® was established and a progressive damage constitutive model was implemented to simulating the impact damage of composite laminates in a user-defined material model (VUMAT) with the consideration of strain rate effects. Hashin and Hou failure criteria was used as the damage initiation criteria, and Murakami-Ogino damage theory was utilized the to establish a damage evolution model for stiffness reduction. Two element deletion methods were parallelly used to delete failed elements. In the simulation model, CFRP and KFRP were in a double-layer stacking form, and the Kevlar fiber mass fraction was determined to be 25%. Numerical tests were conducted on the laminate with different thicknesses (1mm-19mm) impacted by titanium alloy bullet with high velocity from both front and rear sides to study the mechanism of aforementioned thickness effect.

2. Experimental methodology

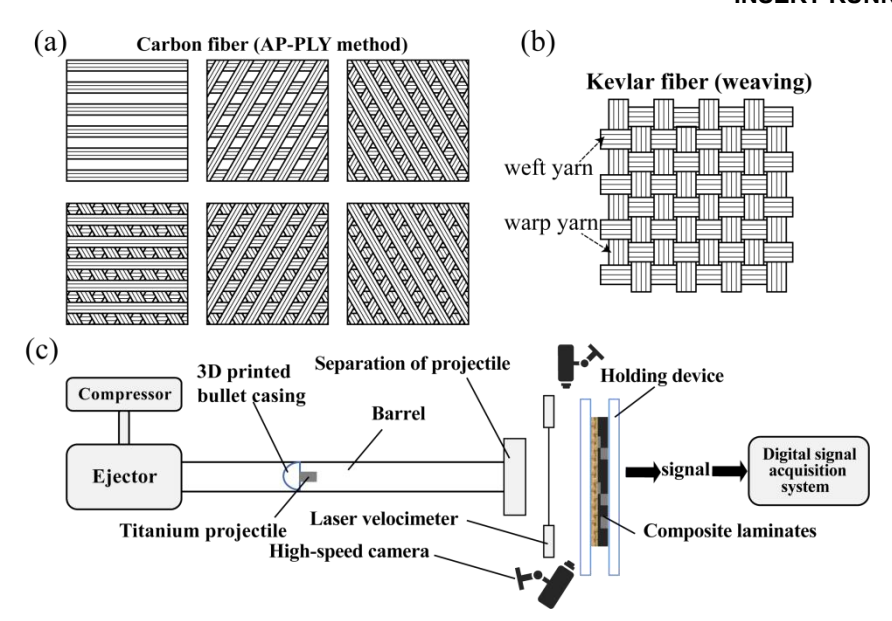


Figure 1 – Schematic diagram of laying method and ballistic impact test.

The hybrid composite being investigated consists of CFRP and KFRP. The CFRP, a carbon fiber reinforced epoxy composite, is created using T800-12K/603B prepreg from Toray Industries, Inc. The KFRP, a Kevlar fiber reinforced epoxy composite, is prepared using F-368 prepreg from China Bluestar Chengrand Co., Ltd. The CFRP is laid out using the Advanced Placed Ply (AP-PLY) method, a novel three-dimensional Automated Fiber Placement (AFP) technology that allows for customized placement paths. As depicted in Figure 1(a), the CFRP is laid out using fiber prepreg tapes in the [\pm 60°/0°] layup directions, each with a width of 50.8 mm, woven in accordance with the AP-PLY method, ensuring a uniform distribution of fibers across -60°, +60°, and 0° directions. The Kevlar fabric (0°/90°) laminate is stacked with prepreg in the 0° direction in Figure1(b). Following the layup, the prepreg and epoxy resin are cured using an autoclave curing process under high pressure (>0.6MPa) and high temperature (>150°C) conditions, resulting in a monolayer thickness of 0.159 mm for CFRP and 0.12 mm for KFRP, respectively.

Ballistic impact experiments were conducted on CFRP/KFRP laminates with different hybrid configurations to determine penetration thresholds and assess impact damage responses. The experimental setup is depicted in Figure 1(c). By controlling the chamber pressure of an 80mm caliber gas gun, the TC4 titanium alloy projectiles were accelerated to a velocity adequate for plate penetration. These high-velocity projectiles impacted the hybrid composite plate, replicating the scenario of engine blade debris colliding with engine case. To maintain data fidelity, each projectile, measuring 50mm × 50mm × 6mm with the 6mm side designated as the impact surface, was standardized at 65.5±1g and utilized singularly.

3. Finite element analysis

3.1 Progressive damage model for composite laminates

To establish a finite element model for composite laminates, it is essential to select a proper constitutive model. In this paper, a progressive damage constitutive model is adopted, which can accurately simulate the initiation and evolution of damage in composite laminates by developing a custom subroutine VUMAT in ABAQUS. The model can be divided into four stages: undamaged stage, damage initiation, damage evolution, and element deletion. If the failure of an element is identified, the stiffness of the element will linearly decrease to zero, and then the element is deleted.

3.1.1 Linear elastic phase

The orthotropic elastic constitutive model of composite material at undamaged stage has been established, and the stress-strain relationship is as follows:

$$\begin{bmatrix}
\sigma_{11} \\
\sigma_{22} \\
\sigma_{33} \\
\sigma_{12} \\
\sigma_{23} \\
\sigma_{31}
\end{bmatrix} = \begin{bmatrix}
C_{11} & C_{12} & C_{13} & 0 & 0 & 0 \\
C_{21} & C_{22} & C_{23} & 0 & 0 & 0 \\
C_{31} & C_{32} & C_{33} & 0 & 0 & 0 \\
0 & 0 & 0 & G_{44} & 0 & 0 \\
0 & 0 & 0 & 0 & G_{55} & 0 \\
0 & 0 & 0 & 0 & G_{66}
\end{bmatrix} \begin{bmatrix}
\varepsilon_{11} \\
\varepsilon_{22} \\
\varepsilon_{33} \\
\varepsilon_{13} \\
\varepsilon_{23} \\
\varepsilon_{31}$$
(1)

where the elastic stiffness constants are defined as follows:

$$\begin{split} &C_{11} = E_{1} \big(1 - v_{23} v_{32} \big) \Gamma \\ &C_{22} = E_{2} \big(1 - v_{13} v_{31} \big) \Gamma \\ &C_{33} = E_{3} \big(1 - v_{12} v_{21} \big) \Gamma \\ &C_{12} = C_{21} = E_{1} \big(v_{21} + v_{31} v_{23} \big) \Gamma \\ &C_{23} = C_{32} = E_{2} \big(v_{32} + v_{12} v_{31} \big) \Gamma \\ &C_{13} = C_{31} = E_{1} \big(v_{31} + v_{21} v_{32} \big) \Gamma \\ &C_{44} = G_{12} \\ &C_{55} = G_{23} \\ &C_{66} = G_{13} \end{split}$$

where the definition of Γ is:

$$\Gamma = 1/(1 - v_{12}v_{21} - v_{23}v_{32} - v_{13}v_{31} - 2v_{21}v_{32}v_{13})$$
(3)

3.1.2 Damage initial phase

Hashin failure criterion and Hou failure criterion are employed to determine the damage caused by fiber tension and compression and the damage caused by matrix tension and compression in this paper, respectively. The initiation criteria for each type of failure mode are provided by the following formulas.

Fiber tension failure $(\sigma_{11} > 0)$:

$$r_{\text{ft}} = \left(\frac{\sigma_{11}}{X_{\text{T}}}\right)^2 + \alpha \left(\frac{\sigma_{12} + \sigma_{13}}{S_{12}}\right)^2 \ge 1$$
 (4)

Fiber compression failure ($\sigma_{11} < 0$):

$$r_{fc} = \left(\frac{\sigma_{11}}{X_C}\right)^2 \ge 1 \tag{5}$$

Matrix tension failure ($\sigma_{22} > 0$):

$$r_{\text{mt}} = \left(\frac{\sigma_{22}}{Y_{\text{T}}}\right)^2 + \left(\frac{\sigma_{12}}{S_{12}}\right)^2 + \left(\frac{\sigma_{23}}{S_{23}}\right)^2 \ge 1$$
 (6)

Matrix compression failure $(\sigma_{22} < 0)$:

$$r_{mc} = \frac{1}{4} \left(\frac{-\sigma_{22}}{S_{12}} \right)^2 + \frac{Y_C^2 \sigma_{22}}{4S_{12}^2 Y_c} - \frac{\sigma_{22}}{Y_c} + \left(\frac{\sigma_{12}}{S_{12}} \right)^2 \ge 1$$
 (7)

where, r_{ft} , r_{fc} , r_{mt} , r_{mc} are the failure criterion values corresponding to the description of damage caused by fiber tension, fiber compression, matrix tension, and matrix compression, respectively. The coefficient α is used to describe the contribution of shear stress to fiber tension failure ($0 < \alpha < 1$). XT, XC, YT, YC denote the longitudinal tensile and compressive strengths, as well as the transverse tensile and compressive strengths of unidirectional laminated composites, whereas S12 and S23 represent the longitudinal and transverse shear strengths, respectively. The values of XT, XC, YT, YC, S12 and S23 were obtained through quasi-static testing. In actual simulation calculations, the strain rate effect of the material under high strain rate loading needs to be considered. The strength of composite material unidirectional laminates under the influence of strain rate effect in all directions can be expressed uniformly as:

$$S = S_0 \left(1 + C \ln \frac{|\dot{\epsilon}|}{\dot{\epsilon}_0} \right) \tag{8}$$

Herein, S represents the strength under the current strain rate ε, S₀ represents the strength under the reference strain rate quasi-static ε_0 , and C is the strain rate hardening correction factor. Carbon fiber composite materials are not sensitive to strain rate and C is taken at the level of 10^{-2} , while Kevlar fibers have strong rate dependence and C is taken at the level of 10^{-1} .

3.1.3 Damage evolution

The process of damage evolution in materials is essentially the release of strain energy. When the strain energy release density equals fracture energy density, it means that the material has completely failed at this point. During the process of strain energy release, the material will soften, revealed as a degradation of the elastic modulus and a decrease in load-carrying capacity. During the damage evolution stage, the degree of stiffness degradation of the material is represented by the damage state variable d. Therefore, the stress-strain relationship of damaged material, including the damage effect, can be modified as [19]:

$$\sigma = C(d)\varepsilon \tag{9}$$

where

$$C(d) = \frac{1}{\Delta} \begin{bmatrix} d_f E_{11} (1 - d_m v_{23} v_{32}) & d_f d_m E_{11} (v_{21} + v_{23} v_{31}) & d_f E_{11} (v_{31} + v_{21} v_{32}) \\ & d_m E_{22} (1 - d_f v_{13} v_{31}) & d_m E_{22} (v_{32} + d_f v_{12} v_{31}) \\ & & E_{33} (1 - d_f d_m v_{12} v_{21}) \\ & & d_f d_m G_{12} \\ & & d_m G_{23} \\ \end{bmatrix}$$
 (10)

$$d_{f} = (1 - d_{ft})(1 - d_{fc})$$
(11)

$$d_{\rm m} = (1 - d_{\rm mt})(1 - d_{\rm mc}) \tag{12}$$

$$d_{m} = (1 - d_{mt})(1 - d_{mc})$$

$$\Delta = \frac{1}{1 - d_{f}d_{m}v_{12}v_{21} - d_{m}v_{23}v_{32} - d_{f}v_{13}v_{31} - 2d_{f}d_{m}v_{21}v_{32}v_{13}}$$

$$(12)$$

In the above equations, d_f is the damage state variable in the fiber direction, d_m is the damage state variable in the matrix direction, and they are related to the damage state variables corresponding to the four in-plane damage modes. According to Murakami-Ohno's damage theory, the damage evolution law for each failure mode I is established from the beginning of loading to complete failure of the material, as follows [20]:

$$d_{I}(\tau) = \max_{\tau} \left\{ 0, \min \left\{ d^{*}, \frac{\epsilon_{I,eq}^{f} \left(\epsilon_{I,eq} (\bar{\tau}) - \epsilon_{I,eq}^{0} \right)}{\epsilon_{I,eq} (\bar{\tau}) \left(\epsilon_{I,eq}^{f} - \epsilon_{I,eq}^{0} \right)} \right\} \right\}, \quad I \in (ft, fc, mt, mc)$$

$$(14)$$

where ∀т≤т. d₁(т) represents the damage state variable corresponding to four in-plane damage modes in finite element simulations at a certain time τ . The use of the max function to express $d_1(\tau)$ indicates that the damage evolution is irreversible. Prior to the initiation of damage, $d_I = 0$, indicating that the material is undamaged. When complete failure occurs, $d_1 = d^*$, where theoretically $d^* = 1$. To avoid singularity in the stiffness matrix calculation in finite element analysis, d^* is set to 0.99. $\epsilon_{l,\rm eq}(\tau)$ represents the current equivalent strain, and the equivalent strains and stresses for each failure mode are calculated using the formulas in Table 1.

Table 1 – Equivalent displacement and equivalent stress of each failure mode.

Failure modes	Equivalence displacement	Equivalence stress		
Fiber tension	$\epsilon_{\text{ft,eq}} = l_{\text{c}} \sqrt{\left(\epsilon_{11}\right)^2 + \alpha\epsilon_{12}^2 + \alpha\epsilon_{31}^2}$	$\sigma_{\text{ft,eq}} = \frac{l_c(\langle \sigma_{11} \rangle \langle \epsilon_{11} \rangle + \alpha \sigma_{12} \epsilon_{12} + \alpha \sigma_{31} \epsilon_{31})}{\epsilon_{\text{ft,eq}}}$		

$$\begin{aligned} & \text{Fiber compression} & \epsilon_{fc,eq} = l_c \langle -\epsilon_{11} \rangle & \sigma_{fc,eq} = \frac{l_c \langle -\sigma_{11} \rangle \langle -\epsilon_{11} \rangle}{\epsilon_{fc,eq}} \\ & \text{Matrix tension} & \epsilon_{mt,eq} = l_c \sqrt{\left\langle \epsilon_{22} \right\rangle^2 + \epsilon_{12}^2 + \alpha \epsilon_{23}^2} & \sigma_{m,eq} = \frac{l_c \left(\left\langle \sigma_{22} \right\rangle \langle \epsilon_{22} \right\rangle + \sigma_{12} \epsilon_{12} + \sigma_{23} \epsilon_{23} \right)}{\epsilon_{mt,eq}} \\ & \text{Matrix compression} & \epsilon_{mc,eq} = l_c \sqrt{\left\langle -\epsilon_{22} \right\rangle^2 + \epsilon_{12}^2} & \sigma_{mc,eq} = \frac{l_c \left(\left\langle -\sigma_{22} \right\rangle \langle -\epsilon_{22} \right\rangle + \sigma_{12} \epsilon_{12} \right)}{\epsilon_{mc,eq}} \end{aligned}$$

In Table 1, the characteristic length of an element l_c is used in the finite element simulation of material failure. If elements of different sizes follow the same constitutive relationship, then the energy release rate during the damage evolution process is proportional to the element size, rather than the area of the fracture surface. By using the crack band model, the characteristic length of an element (the cube root of the volume of a solid element) is introduced into the damage evolution expression, which expresses the constitutive relationship of the element material as a stress-displacement relationship and reduces to some extent the dependence of the energy release rate on the mesh during the material softening process. The dissipated energy of element $G_{\rm I}$ can be expressed as:

$$G_{\rm I} = \frac{1}{2} \sigma_{\rm eq}^{\rm f} \varepsilon_{\rm eq}^{\rm f} l_{\rm c} \tag{15}$$

In Eq. (14), $\epsilon_{I,eq}^f$ is represents the fully failed equivalent strain of the corresponding failure mode, while $\epsilon_{I,eq}^0$ represents the initial equivalent strain that satisfies the failure criterion. These two values can be calculated using the following formulas:

$$\begin{split} \epsilon_{l,eq}^f &= \frac{2G_I}{\sigma_{l,eq}^0} \\ \epsilon_{l,eq}^0 &= \epsilon_{l,eq} \Big|_{r_t=1} \end{split} \tag{16}$$

3.1.4 Element deletion

This paper employs two parallel methods for deleting laminate elements as the criterion. When the criterion is met, the variable controlling the effective state of the material is set to 0, indicating failure. The first criterion for element deletion is based on the damage variable $d_{\rm I}$ of the element. Theoretically, when $d_{\rm I}=1$, the element fails completely and is removed. The second criterion for element deletion is based on the degree of distortion of the element. For explicit dynamic analysis such as impact, severe deformation of the element will cause the calculation process to terminate, so highly distorted elements can be deleted. The degree of distortion of the element is evaluated by the distortion parameter eMax, which characterizes the deformation gradient of the element. To establish a finite element model for composite laminates, it is essential to select a proper constitutive model. In this paper, a progressive damage constitutive model is adopted, which can accurately simulate the initiation and evolution of damage in composite laminates by developing a custom subroutine VUMAT in ABAQUS. The model can be divided into four stages: undamaged stage, damage initiation, damage evolution, and element deletion. If the failure of an element is identified, the stiffness of the element will linearly decrease to zero, and then the element is deleted.

3.2 Finite element model

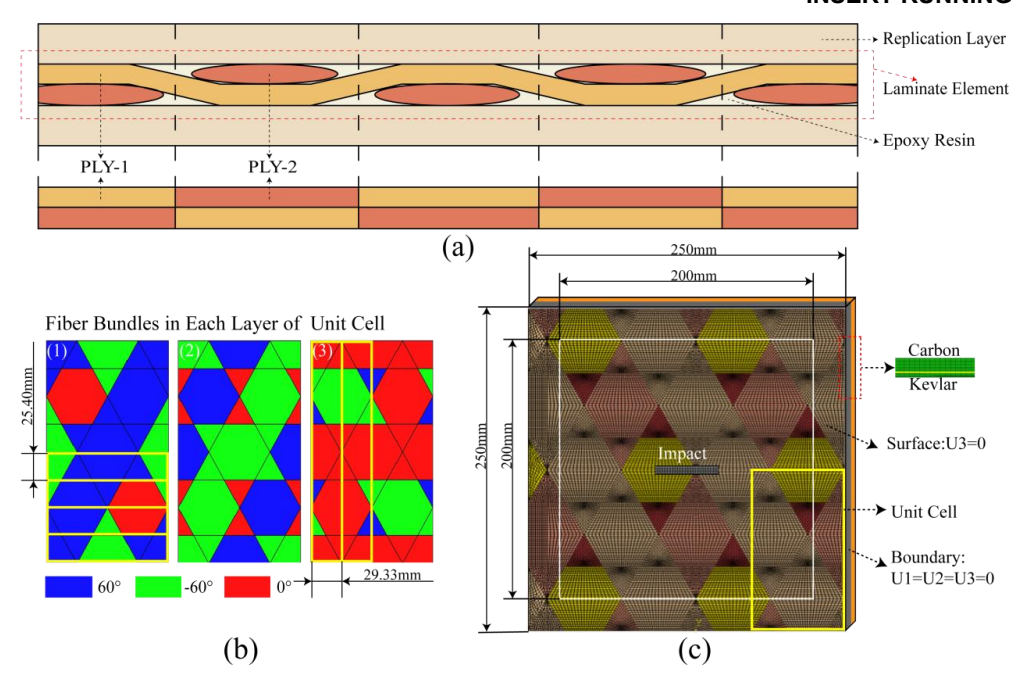


Figure 2 – Finite element model of the hybrid composite laminates.

As shown in Figure 2(c), in the ballistic impact simulation experiment, Composite plates are composed of carbon fiber layers and Keylar fiber layers of different thicknesses, with a size of 250 mm × 250 mm. For carbon fiber laminates, the mesh division is based on the simplified twodimensional AP-PLY method. The simplified mesh can be understood as the squeezed prepregs that are arranged at intervals, and each layer will have components of other compressed layers. Therefore, the unit cell constructed in Hypermesh®, contains fiber bundles at 0°, 60°, and -60° in each layer of the mesh, as shown in Figure 2(a). The CFRP meshed laminated plate is extended and spliced by the unit cell, consisting of three layers, each with a thickness of 0.159mm. For Kevlar fiber laminates, the overall 0° layup is adopted. The meshing method is same as that for carbon fiber laminates for modeling convenience. The element type is C3D8R element, with a size of 1.4mm × 1.8mm, and the element height is consistent with the single layer thickness. The TC4 bullet is given an initial impact velocity, and the velocity direction is perpendicular to the composite plate. The boundary conditions of the composite plate refer to the set-up of the target plate in the experiment. The front and rear surfaces outside (200mm × 200mm) in Figure 2(c) are constrained in the outward direction, and the degrees of freedom in three directions of the four sides of the target plate are constrained. To validate the accuracy of the CFRP finite element model, subregions of the same size were extracted from different positions of each layer of the cell depicted in Figure 2(b) for for quasi-static loading verification. The quasi-static tensile model of the Kevlar fibers was established with dimensions of 25mm×25mm×2.64mm, while the compression test utilized direct displacement loading with a model size of 12mm×13mm×2.64mm.

4. Comparison and validation of experimental and simulated results

4.1 Comparison and validation under quasi-static conditions

In section 3.2, the finite element model was established, and a subregion for quasi-static loading verification was extracted from the carbon fiber unit cell in Figure 2(b). The simulation results showed that the modulus results of these subregions at different positions were basically consistent, with slight differences in strength, stemming from certain differences in the orientation of carbon fiber bundles at different positions. Ultimately, through averaging calculations, the stiffness and strength results obtained from the carbon fiber simulation were determined. As shown in Table 2, the simulated predictions of the 0° and 90° tensile and compressive modulus and strength were generally consistent with the experimentally measured results. It reflects that the AP-PLY ply layer could effectively simulate woven fibers, ensuring consistency in the tensile results of the laminate in various directions in different regions. Subsequently, the quasi-static simulation of Kevlar fiber-reinforced epoxy composite laminates was compared with experimental results in Table 2, showing errors within an acceptable range. Considering the quasi-static verification results

of both carbon fibers and Kevlar fibers, it can be concluded that the finite element model established in this study can accurately simulate the failure process of composite laminates.

Fiber Type	Quasi-Static Operating Conditions	Experimental Modulus (GPa)	Simulated Modulus (GPa)	Error (%)	Experimental Strength (MPa)	Simulated Strength (MPa)	Error (%)
	0°Tensile	55.3	55.09	0.38	895	718	19.78
O a ula a u	90°Tensile	53.8	53.43	0.69	645	793	22.95
Carbon	0°Compression	49.7	56.01	12.7	565	483	14.51
	90°Compression	48.9	54.87	12.21	569	564	0.88
	0°Tensile	38.3	37.4	2.35	923	866	6.18
Kaylar	90°Tensile	32.3	31.3	3.1	670	590	11.94
Kevlar	0°Compression	32.2	38.2	18.63	180	165	8.33
	90°Compression	29.3	32.2	9.9	172	159	7.56

4.2 Comparison and validation of ballistic impact test and simulation results

Experimental and simulation studies were carried out for titanium alloy impact hybrid composite target plates to compare the critical penetration velocity and damage obtained from experiments and simulations, thereby validating the accuracy of the impact model.

Simulations of target plate impact were conducted on pure carbon fiber and pure Kevlar fiber laminates, with the similarity between the critical penetration velocity obtained from simulations and experiments serving as the basis for parameter tuning. Ultimately, the distortion parameters for the carbon fiber composite laminate were adjusted to CeMax=0.07, while the Kevlar fiber composite laminate's distortion parameters were set to KeMax=0.33 and the strain rate effect coefficient CK=0.18. To validate the accuracy of these parameters, impact tests were performed on target plates with a hybrid stacking sequence of front and rear layers. For the Kevlar fiber composite laminate, serving as the impact surface with a mass fraction of 25% and a thickness of 8.5mm, after multiple tests, the critical penetration velocity was determined to be between 173m/s and 174m/s. Corresponding simulation models were established in Abaqus, yielding a critical penetration velocity range of 172m/s to 177m/s. As shown in Figure 4, The small deviation from the experimental results indicates a high level of accuracy. The critical penetration velocity results to some extent validate the ability of the simulation model to accurately simulate the target plate impact of hybrid fiber laminates.

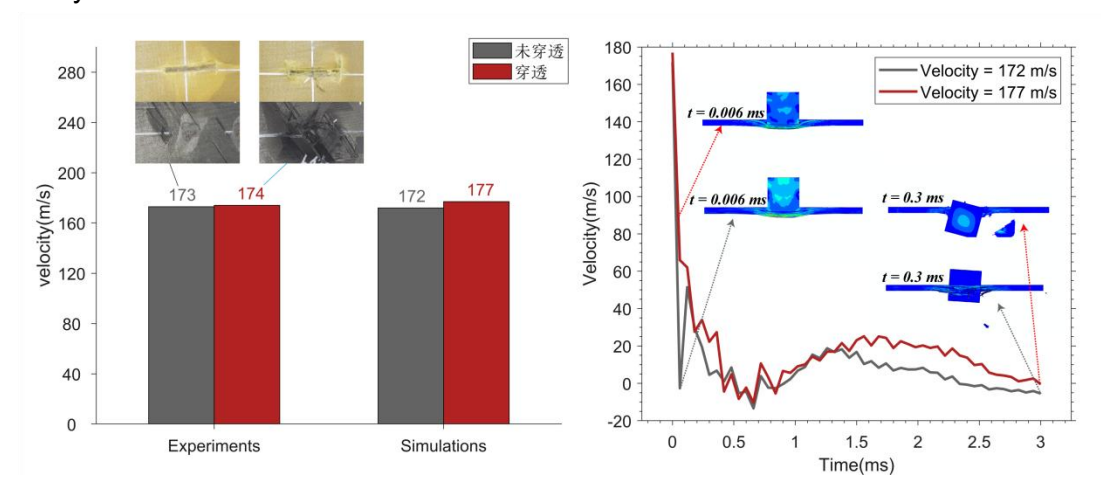


Figure 4 – Comparison of ballistic impact test and simulation results.

Furthermore, we conducted impact experiments and simulations on hybrid laminates with different structures and a mass fraction of 35%. Experimental results are shown in Figure 5. The impact surfaces exhibit smooth and continuous damage across the penetration, with the damaged area closely resembling the size of the bullet's impact area. On the back surface, there is evident tensile fracture, significant matrix cracking, and fiber debonding. The results are summarized in Table 3, indicating excellent agreement between experimental and simulated results. C means [±60°/0°]CFRP

and K means a layer of KFRP. C in front and K behind means a plate with CFRP on the impact side and KFRP on the back side, and vice versa.

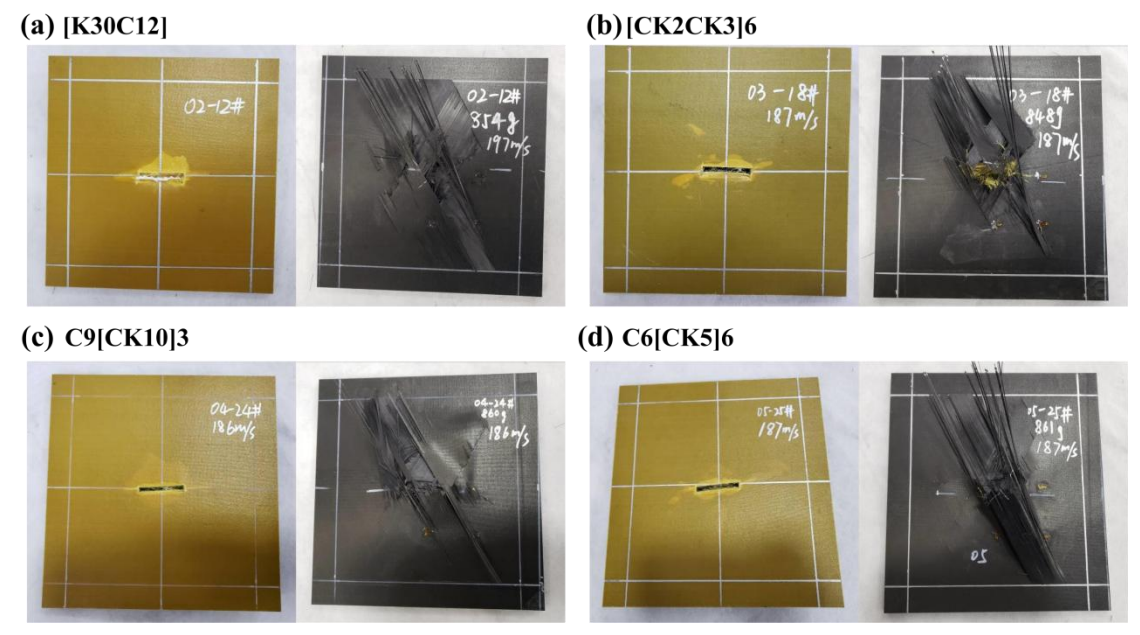


Figure 5 – Impact results of target plates with different hybrid sequences. Table 3 - Ply stacking sequences of nine multi-phase composite laminates

	Construction	Stacking sequence	Experimental velocity (m/s)	Simulation velocity(m/s)	Error(%)
1	$C_{12}K_{30}$	$[\pm 60/0]_{12}K_{30}$	187-197	190-195	3.2
2	$C_{12}K_{30}$	$[(\pm 60/0)K_2(\pm 60/0)A_3]_6$	182-187	185-190	0.5
3	$C_{12}K_{30}$	$(\pm 60/0)_9[(\pm 60/0)K_{10}]_3$	185-186	185-190	2.1
4	$C_{12}K_{30}$	$(\pm 60/0)_6[(\pm 60/0)K_5]_6$	183-187	185-192	3.2

After validating the accuracy of the model, it is possible to carry out numerical simulations of

5. Critical penetration velocity of hybrid laminates with different configurations

impact experiments on hybrid fiber laminates under various conditions based on this foundation. Setting the Kevlar mass fraction at 25%, with CFRP and KFRP serving as the impact surfaces respectively, to investigate the relationship between critical penetration velocity and thickness variation under these two conditions. Figure 6 presents the critical penetration velocities obtained from numerical simulations of hybrid composite target plates containing 25% Kevlar fibers layer. The blue curve represents the Kevlar fiber layer as the impact surface, while the red curve represents the carbon fiber layer as the impact surface. It can be observed that for the target plate with a 25% Kevlar mass fraction, the critical penetration velocity ranges from approximately 150-160 m/s when the target plate thickness is around 8 mm, regardless of whether the carbon or Kevlar fiber layers serve as the impact surface. When the thickness is less than 8 mm, the target plate exhibits a higher resistance to impact when the Kevlar fiber layers serve as the backing surface, while when the thickness is greater than 8 mm, the opposite conclusion is reached. The simulation results confirm the thickness effect on the ballistic impact behavior of the hybrid composite laminate, whereby the hybrid composite laminates exhibit superior impact resistance when Kevlar fiber layers serving as the backing surface for thinner plates, while the opposite is true for thicker plates.

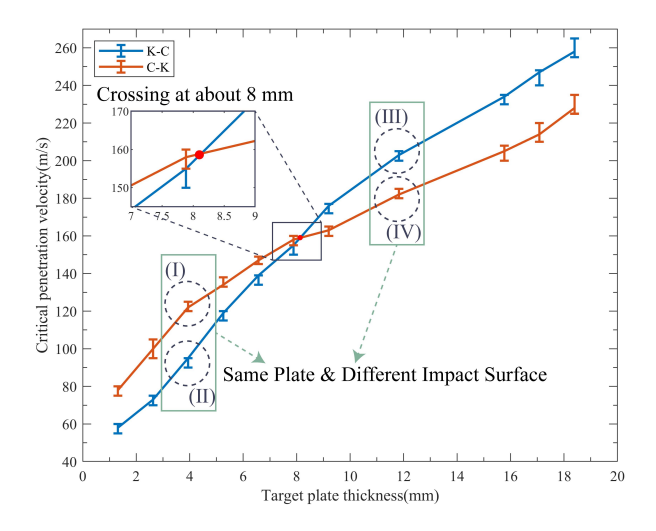


Figure 6 – Critical penetration velocity versus thickness for different impact surfaces

For the Kevlar fiber layer as the back face of the target plate, the growth of critical penetration velocity slows down as the thickness of the target plate increases, especially when its thickness is greater than 5mm. Therefore, it is reasonable to speculate that the energy absorption mechanism of the target plate with Kevlar fiber layer as the back face changes with the increase of thickness. As the thickness reaches a certain value, the macroscopic damage form changes significantly. Four typical cases are labeled in Figure 6, including (I)[±60°/0°]₆K₉(C-K), (II)K₉[±60°/0°]₆(K-C), (III)[±60°/0°]₁₈K₂₇(C-K), and (IV)K₂₇[±60°/0°]₁₈(K-C). Cases (I) and (II) essentially share the same target structure with a thickness of 3.94 mm, defined as thin plate. The impact surface of case (I) is made of carbon fiber, while the impact surface of case (II) is made of Kevlar fiber. Similarly, cases (III) and (IV) have the same target structure with a thickness of 11.83 mm, defined as thick plate. Consistent with most literature [19-23], the Kevlar fiber layer located at the back surface of the thin plate (I) exhibits better impact resistance than that of case (II). The simulation results show that the critical penetration velocity of case (I) is 30 m/s higher than that of case (II). In contrast, the opposite is observed for cases (III) and (IV), where the critical penetration velocity of the carbon fiber located at the back surface of the thick plate (IV) is 30 m/s higher than that of case (III). Further analysis of the mechanism behind this phenomenon will be conducted in the following sections.



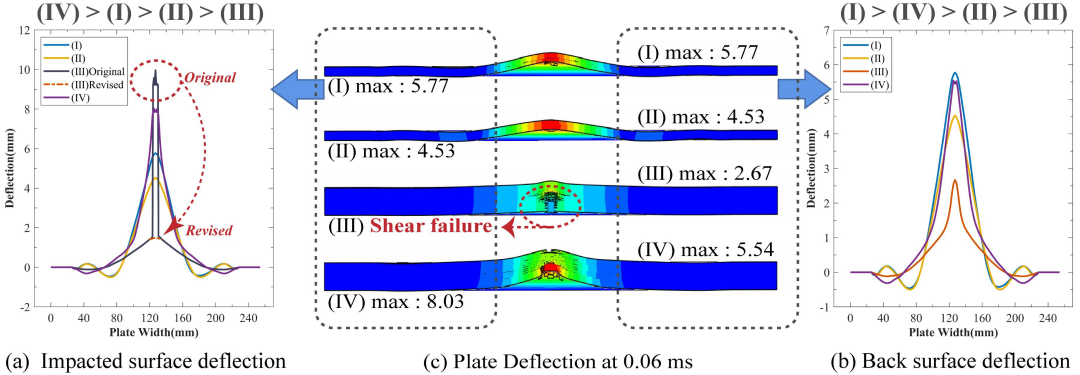


Figure 7 – Distribution of central deflection in the width direction of the plate at 0.06ms. (a) Impacted surface deflection; (b) Back surface deflection; (c) plate at 0.06ms

Figure 7 depicts the central cross-sectional profile of the target plate under critical penetration velocity, which reflects the distribution of deflection on the impacted and non-impacted surfaces along the width direction of the plate. By comparing the two subfigures (a) and (b), it can be observed that the expansion of the thin plates (I) and (II) is harmonious, with consistent deflection changes and bending deformations. The maximum deflection of the thin plate (I) with Kevlar fiber

layer at the back is larger, and the deflection changes in the front and back of the plate are both 5.77 mm. It can be inferred that the thin plate (I) with Kevlar fiber serving as the back expands more, fully utilizing its good ductility and high fracture elongation characteristics. When subjected to impact, they absorb a large amount of energy without fracturing, resulting in a better impact resistance of the thin plate (I) than (II).

As expected, the maximum deflections of the impacted surface and back surface of thick plates are not consistent at the same moment, as thick plates have greater bending stiffness compared to thin plates. With increasing thickness, the bending resistance increases, making it difficult for the thick plate to undergo overall bending deformation before damage occurs. Thicker plates exhibit smaller ranges of deflection variation compared to thinner plates, and when subjected to impact, the tensile region behind the thick plate is much smaller than that behind the thin plate, resulting in more localized damage. The impacted surface of thick plate III is composed of carbon fibers, as shown in Figure 7 (a), and the original simulation data shows a very large deflection value. However, this is not an actual deformation value as the carbon fibers on the impacted surface undergo shear damage almost immediately upon impact, resulting in the detachment of broken carbon fibers and the large deflection values are due to the detachment of damaged carbon fibers on the bullet impact surface. The back surface of thick plate III is made of Kevlar fibers and undergoes minimal deformation, with a maximum value of 2.67mm, slightly larger than the corrected deflection value of the impacted surface carbon fibers, as shown in Figure 7 (b). The back of thick plate III only has a slight bulge, indicating that the braking of the Kevlar fibers on the back surface is not the main energy absorption mechanism. For thick plate IV, the deflection value of the impacted surface Kevlar fibers is 8.03mm, much larger than the deflection value of the back surface carbon fibers of 5.54mm, indicating that the instantaneous compression and depression of the Kevlar fiber layer on the impacted surface has a certain energy absorption effect, which can be understood as a cushioning layer that disperses stress waves and reduces tensile deformation on the back surface.

The deflection results indicate that the maximum deflection occurs during the impact moment in the (I) C-K thin plate, followed by the (IV) K-C thick plate, (II) K-C thin plate, and (III) C-K thick plate in sequence. Furthermore, according to the simulation results of the critical penetration velocity, it is found that the (I) and (IV) configurations are the optimal impact-resistant solutions for the two thicknesses, corresponding to the structures with the maximum deflection in each case. The larger deflection indicates greater deformation with fibers and matrix, suggesting that the energy absorbed by tensile deformation accounts for a significant portion of the impact energy. As the (I) and (IV) configurations exhibit greater tensile deformation, their critical penetration velocities are higher, demonstrating superior impact resistance.

5.2 Damage of four typical cases with different configurations

The damage evolution for the target plates with C-K configurations (Cases I and III) is shown in Figure 8. For the thin plate (Case I) at an instantaneous impact at 0.06 ms, there is significant overall tensile deformation. The CFRP laminate at the impact surface suffers minor damage, and the KFRP laminate on the back remains largely intact. Subsequently, the damage progresses from the CFRP laminate to the KFRP laminate, leading to separation of the two materials. In contrast, the thick plate (Case III) exhibits a three-stage progression of damage: (1) minimal deformation and shear damage to most of the CFRP laminate at the impact surface, (2) complete penetration of the CFRP laminate followed by expansion and damage to the KFRP laminate, and (3) full fracture of the KFRP laminate with clear material separation. The main difference between the two cases is that the thick plate in Case III undergoes a significant shear plugging stage, during which most of the CFRP laminate on the impact surface undergoes instantaneous shear failure, exhibiting clear shear fracture surfaces with almost no bending deformation occurring in the region with shear plugging. It can be observed that an increase in plate thickness correlates with a notable reduction in matrix tensile failure for the CFRP laminate on the impact side of the plate. This finding is attributed to the overall expansion deformation of the thin plate (Case I), which leads to a larger area of damage to the CFRP laminate on the impact side. A portion of the impact energy is dissipated through carbon fiber matrix failure, contributing to an enhanced ballistic limit. In contrast, the CFRP laminate on the impact side on the thick plate (Case III) undergoes shear plugging,

limiting the absorption of energy due to the smaller amount of matrix damage.

The damage evolution for the K-C configurations (Cases II and IV) is also shown in Figure 8. Compared to the laminate with Kevlar fiber, which has high ductility, the laminate with carbon fiber is more prone to fracture upon impact when used as the back face of the target plate. At an instantaneous impact of 0.06 ms, no significant damage to the KFRP laminate at the impact surface can be noted for the thin plate (Case II), whereas the CFRP laminate at the back side undergoes tensile failure. For the thick plate (Case IV) at the moment of impact, the KFRP laminate at the impact surface deforms considerably, acting as a cushioning layer that disperses stress waves and reduces tensile deformation at the back side of the plate. Initial tensile failure occurs in the outermost CFRP layer.

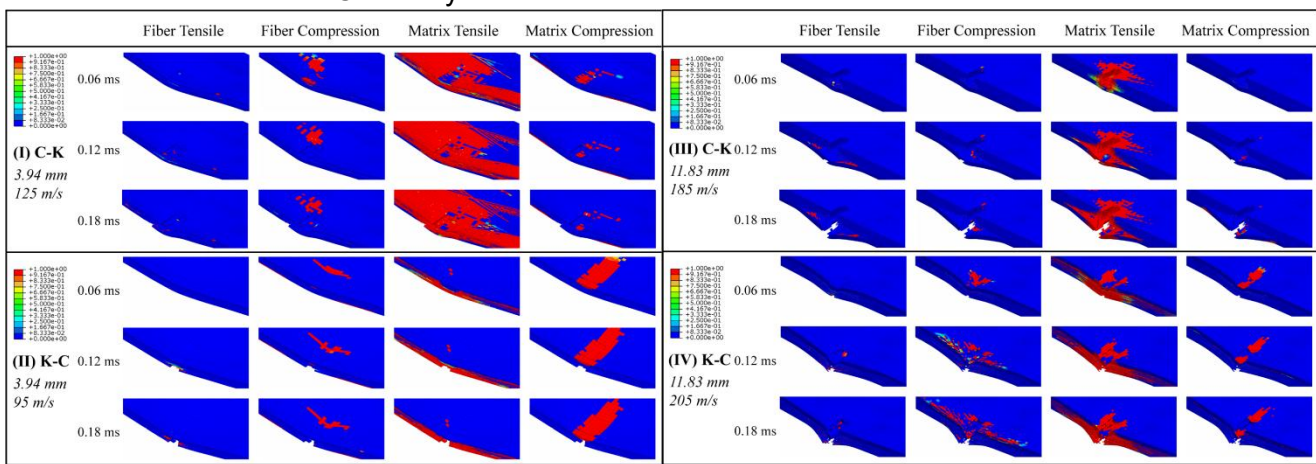


Figure 8 – Numerical damage contours of four typical laminates for projectile impacting at critical penetration velocity

5.3 Shear plugging Impact mechanisms of four hybrid composite laminates Kevlar Carbon Integral flexion, Damage Larger damage area (a) Thin-C-K (b) Thin-K-C Similar Different mechanisms mechanisms local buffering Disengagement Backside damage Shear plugging, Complete fracture: Smaller damage area Internal occurrence (c) Thick-C-K (d) Thick-K-C **CONCLUSION:** The C-K laminate has stronger impact resistance when the thickness is thin, while the K-C laminate has stronger impact resistance when the thickness is thick.

Figure 9 – Impact damage mechanisms of four hybrid composite laminates with different thicknesses and impact surfaces.

The thickness effect is mainly due to variations in the damage mechanisms for the plates with C-K configurations. As shown in the diagram Figure 9, as the thickness increases, the damage to the CFRP laminate in the plates with C-K configurations changes from tensile failure in the thin plate (Figure 9(a)) to shear plugging in the thick plate (Figure 9(c)), reducing the size of the damaged area and the energy absorption efficiency. In contrast, the plates with K-C configurations exhibit consistent damage mechanisms. Concurrently, the KFRP laminate on the impact surface

undergoes progressive failure, while the CFRP laminate on the back surface undergoes tensile failure from the outermost to the inner layers. Ultimately, a complete fracture occurs within the interior of the target plate. The transition between these two stages is a complex phenomenon, but it can be characterized by the shear plugging ratio.

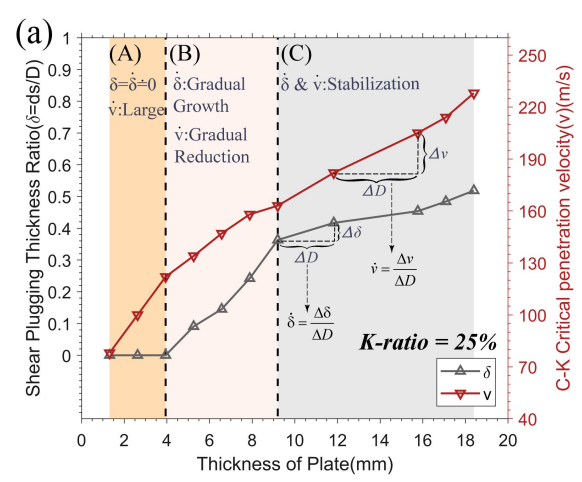


Figure 10 – The relationship between shear plugging and critical penetration velocity versus plate thickness

With increasing thickness, the target plate exhibits enhanced resistance to bending deformation. Upon reaching a sufficient thickness, there is a notable change in the failure mechanism of the plates with C-K configurations. While the characterization of this change is multifaceted, the shear plugging part is relatively perceivable, since the carbon fiber layers that undergo shear plugging remain essentially unbent. Therefore, the ratio of the shear plugging thickness to the total thickness, denoted by δ , can be easily calculated. As shown in Figure 10, with the increase of the thickness of a plate with the C-K configuration, the shear plugging thickness ratio δ increases. Moreover, the growth rate of shear plugging ($\dot{\delta}$) and the growth rate of critical penetration velocity (\dot{v}), show a negative correlation. The increasing trend in the shear plugging ratio agrees well with the critical penetration velocity, elucidating the reasons for the thickness effect. As the thickness increases, the CFRP laminate on the impact surface of a plate with a C-K configuration exhibits a progressively higher amount of shear plugging. Consequently, the energy absorption via tensile deformation decreases, resulting in a decline in both the energy absorption capacity and the impact resistance of the thicker laminate.

6. Conclusions

To sum up, this study investigates the impact damage behavior of carbon/Kevlar hybrid fiber-reinforced composite laminate through ballistic impact tests and finite element models based on progressive damage constitutive equations. The accuracy of the finite element model in predicting the impact resistance and damage behavior of hybrid composites was verified by quasi-static tests and ballistic impact tests. Different thicknesses (1mm-19mm) of target plates with carbon and Kevlar fiber layers serving as the impact face were simulated to analyze the impact damage behavior and critical penetration velocity under different conditions. The following remarks can be concluded:

- 1. Thickness effect significantly affects the impact resistance of hybrid composite laminates with different back faces. Regarding the hybrid composite laminates with the 25% Kevlar fiber mass fraction, Kevlar fiber layers as the back face have stronger impact resistance when the thickness is thin, while carbon fiber layers as the back face have stronger impact resistance when the thickness is thick.
- 2. The energy absorbed by tensile deformation accounts for a significant portion of the impact energy. Thin plates are more suitable for placing Kevlar fibers at the back face to fully utilize their high fracture elongation. Thicker plates have greater bending stiffness and are less likely to undergo overall bending deformation before damage occurs, resulting in a reduction in energy absorbed by tensile deformation.

- 3. When Kevlar fiber layers are used as the back face of the target plate, large expansion deformation occurs in thin plates, absorbing energy and undergoing tensile failure. In thicker plates, the damage can be divided into three stages. In the first stage, a shear plug phenomenon occurs, which is not present in thin plates. Some carbon fibers that the bullet contacts first undergo penetrative shear failure without significant deflection (<2mm). In the subsequent second and third stages, both carbon and Kevlar fibers undergo tensile failure.
- 5. The shear plugging phenomenon of carbon fibers causes the thickness effect. Carbon fibers that undergo shear failure do not experience bending deformation. As the thickness of the laminate increases, the ratio of shear plugging thickness to the laminate thickness increases, and the ability of carbon fiber matrix tensile failure elements to absorb impact energy decreases significantly.

With this information, optimal hybridization laminate can be designed for different thicknesses, which can be used to guide the design and optimization of areo-engine cases in practical engineering applications.

Contact Author Email Address

E-mail: celluloid2@mail.nwpu.edu.cn

Copyright Statement

The authors confirm that they, and/or their company or organization,hold copyright on all of the original material included in this paper. The authors also confirm that they have obtained permission, from the copyright holder of any third party material included in this paper, to publish it as part of their paper. The authors confirm that they give permission, or have obtained permission from the copyright holder of this paper, for the publication and distribution of this paper as part of the ICAS proceedings or as individual off-prints from the proceedings.

References

- [1] Liu L, Cai M, Liu X, Zhao Z, Chen W. Ballistic impact performance of multi-phase STF-impregnated Kevlar fabrics in aero-engine containment. Thin-Walled Structures. 2020;157:107103.
- [2] Roberts GD, Pereira JM, Braley MS, Dorer JD, Watson WR. Design and testing of braided composite fan case materials and components. 19th ISABE Conference (ISABE 2009)2009.
- [3] Marsh G. Aero engines lose weight thanks to composites. Reinforced Plastics. 2012;56:32-5.
- [4] Roberts GD, Revilock DM, Binienda WK, Nie WZ, Mackenzie SB, Todd KB. Impact testing and analysis of composites for aircraft engine fan cases. Journal of Aerospace Engineering. 2002;15:104-10.
- [5] Basha M, Wagih A, Melaibari A, Lubineau G, Eltaher M. On the impact damage resistance and tolerance improvement of hybrid CFRP/Kevlar sandwich composites. Microporous and Mesoporous Materials. 2022;333:111732.
- [6] Gustin J, Joneson A, Mahinfalah M, Stone J. Low velocity impact of combination Kevlar/carbon fiber sandwich composites. Composite structures. 2005;69:396–406.
- [7] Karthick P, Ramajeyathilagam K. Numerical study on ballistic impact behavior of hybrid composites. Materials Today: Proceedings. 2022;59:995–1003.
- [8] Bandaru AK, Vetiyatil L, Ahmad S. The effect of hybridization on the ballistic impact behavior of hybrid composite armors. Composites Part B: Engineering. 2015;76:300–19.
- [9] Hazell PJ, Appleby-Thomas G. A study on the energy dissipation of several different CFRP-based targets completely penetrated by a high velocity projectile. Composite structures. 2009;91:103–9.
- [10] Li Z-y, Xue Y-s, Sun B-z, Gu B-h. Ballistic penetration damages of hybrid plain-woven laminates with carbon, Kevlar and UHMWPE fibers in different stacking sequences. Defence Technology. 2022.
- [11]Tanabe Y, Aoki M, Fujii K, Kasano H, Yasuda E. Fracture behavior of CFRPs impacted by relatively high-velocity steel sphere. International Journal of Impact Engineering. 2003;28:627-42.
- [12]Cheon J, Lee M, Kim M. Study on the stab resistance mechanism and performance of the carbon, glass and aramid fiber reinforced polymer and hybrid composites. Composite structures. 2020;234:111690.
- [13] Grujicic M, Pandurangan B, Koudela KL, Cheeseman BA. A computational analysis of the ballistic performance of light-weight hybrid composite armors. Applied Surface Science. 2006;253:730–45.
- [14] Nguyen LH, Ryan S, Cimpoeru SJ, Mouritz AP, Orifici AC. The effect of target thickness on the ballistic

INSERT RUNNING TITLE HERE

- performance of ultra high molecular weight polyethylene composite. International Journal of Impact Engineering. 2015;75:174–83.
- [15]Gellert EP, Cimpoeru SJ, Woodward RL. A study of the effect of target thickness on the ballistic perforation of glass-fibre-reinforced plastic composites. International Journal of Impact Engineering. 2000;24:445-56.
- [16]Nunes SG, Scazzosi R, Manes A, Amico SC, de Amorim Júnior WF, Giglio M. Influence of projectile and thickness on the ballistic behavior of aramid composites: Experimental and numerical study. International Journal of Impact Engineering. 2019;132:103307.
- [17]Shaktivesh, Nair NS, Sesha Kumar CV, Naik NK. Ballistic impact performance of composite targets. Materials & Design. 2013;51:833–46.
- [18]Naik NK. 14 Ballistic impact behavior of composites: Analytical formulation. In: Silberschmidt V, editor. Dynamic Deformation, Damage and Fracture in Composite Materials and Structures (Second Edition): Woodhead Publishing; 2023. p. 391–439.
- [19] Huang J, Zhang C, Wang J, Zhang C. On the applicability of rate-dependent cohesive zone models in low-velocity impact simulation. Engineering Fracture Mechanics. 2022;271:108659.
- [20]Sitnikova E, Guan Z, Schleyer G, Cantwell W. Modelling of perforation failure in fibre metal laminates subjected to high impulsive blast loading. International Journal of Solids and Structures. 2014;51:3135–46.

15